WAVEFIELD RECONSTRUCTED LEAST-SQUARES REVERSE TIME MIGRATION BASED ON STABLE PURE qP-WAVE EQUATION IN TILTED TRANSVERSELY ISOTROPIC MEDIA

YI DING[1,2], ZHENCHUN LI[1,2], KAI ZHANG[1,2] and YUNYUN SANG[3]

[1] *School of Geoscience, China University of Petroleum, Qingdao 266555, P.R. China. zhksam@163.com*
[2] *Key Laboratory of Deep Oil and Gas, China University of Petroleum (East China), Qingdao 266555, P.R. China.*
[3] *Data Processing Center, Bureau of Geophysical Prospecting INC., China National Petroleum Corporation, Zhuozhou 072750, P.R. China.*

(Received November 17, 2021; revised version accepted March 2, 2022)

ABSTRACT

Ding, Y., Li, Z.C., Zhang, K. and Sang, Y., 2022. Wavefield reconstructed least-squares reverse time migration based on stable pure qP-wave equation in tilted transversely isotropic media. *Journal of Seismic Exploration*, 31: 279-303.

The anisotropy of underground media is an important physical property that affecting the propagation of seismic wave. It generally exists in sedimentary strata. Therefore, this property should not be ignored in the process of exploration seismic imaging. Vertical transversely isotropic (VTI) hypothesis ignores the influence of original stratum tilt on anisotropy. Although it remedies the defect of acoustic hypothesis to a certain extent, it is difficult to accurately describe the propagation of seismic wave in most cases, leading to serious imaging footprints in reverse time migration (RTM) and least-squares reverse time migration (LSRTM) based on two-way wave equation. LSRTM can hardly eliminate them by iterations or denoising in frequency domain. Tilted transversely isotropic (TTI) pseudoacoustic equation is a strategy that can be considered, but the assumption that shear wave velocity is zero brings serious numerical errors to the coupled equation under complex anisotropic conditions. We use a stable pure pseudoacoustic wave equation to simulate wavefield in TTI media and apply it to LSRTM. On this basis, the wavefield reconstruction algorithm in TTI media is further derived to constrain the inversion process of LSRTM. Our algorithm can suppress the artifacts of high-order scattering wave, and accelerate the convergence of objective function. Experiments show that our method can achieve images with high signal-to-noise ratio (SNR) under TTI condition.

KEY WORDS: tilted transversely isotropic media, least-squares reverse time migration, wavefield reconstruction.

0963-0651/22/$5.00

INTRODUCTION

The research on seismic forward modeling and imaging is a process from simple hypothesis to complex hypothesis. The original seismic imaging technologies rely on acoustic approximation and ignore anisotropy. With the deep research and the improvement of computer power, anisotropic assumptions were introduced into seismic forward modeling. The current interest of research is mainly on the transverse isotropic (TI) media, it means that there is a two-dimensional plane in the elastic media, in this plane, the elastic properties remain unchanged. TI media can be divided into three categories: vertical transversely isotropic (VTI) media, horizontal transverse isotropic (HTI) media and tilted transverse isotropic (TTI) media. VTI and HTI are two simple descriptions of anisotropic properties. In VTI media, the isotropic symmetry axis is perpendicular to horizontal plane. Similarly, the isotropic symmetry axis in HTI media is consistent with horizontal direction. However, if the tilt of the symmetry axis is considered, such media is TTI, which are based on the most complex anisotropic hypothesis. The stiffness matrix describing TTI media shows the highest algebraic complexity. If the TTI impact on seismic modeling is not concerned, the image will fail to yield desired results and cause imaging footprints (Uhsenbach and Bale, 2009).

Alkhalifah (2000) creatively realizes the qP-wave propagation in TI media by using acoustic approximation, which ignores the vertical S-wave velocity, and gives the dispersion equation of qP-wave. This research provides a theoretical guidance for anisotropic RTM using only P-wavefield. On this basis, many scholars have deeply studied the forward modeling of wavefield under anisotropic conditions. The initial pseudoacoustic wave equation is a fourth-order equation, which is difficult to calculate. In order to improve the calculation efficiency, Hestholm (2009) and Fletcher et al. (2008) have derived several forms of low-order coupled pseudoacoustic wave equations in VTI media using various order reduction methods, while Duveneck et al. (2008) derived formulas that are more suitable for the actual physical situation based on Hooke's Law and Newton's Second Law. Fowler et al. (2010) gave the general form of the second-order qP-wave equation in VTI media based on the above research results, confirmed the equivalence of such equations, and gave the second-order coupled qP- and qSV-wave equations in VTI media by ignoring S-wave velocity. The equation derivation in TTI media can follow the above method. For example, Zhou et al. (2006) and Fletcher et al. (2009a,b) gave the TTI qSV-wave equation based on the dispersion relationship, and Zhang et al. (2011) proposed stable TTI equations. Duveneck and Bakker (2011) rotated the stress and strain tensor to the local coordinate system aligned with TTI media, made full use of the simple and sparse form of local elastic tensor in VTI media, and obtained a stable coupling equation in TTI media.

However, the above methods based on pseudoacoustic approximate still have defects. The main obstacles in imaging and inversion is the S-wave interference and numerical dispersion. Grechka et al. (2004)

confirmed that this artifact is caused by the pseudo shear wave generated when the shear wave velocity is artificially set to zero, and its wavefront presents the shape of a diamond. The above method also requires Thomsen parameters to meet the condition $\varepsilon > \delta$ to make sure the stable propagation of qP-wave, which increases the instability of numerical calculation.

The initial theoretical basis of the least-squares inversion was proposed by Tarantola et al. (1984). However, due to the limitation of computing resources, the development was quite slow for a long time. Lambaré et al. (1992) introduced the method of least-squares inversion into Kirchhoff migration, and was the first to realize the combination of least-squares inversion theory and seismic imaging. With the improvement of calculating speed and storage capacity, two-way wave migration represented by RTM has become a magnet for researchers. Combined with Tarantola's least-squares inversion theory and Lambaré's imaging framework, Dai and Schuster (2013) optimized RTM to LSRTM, strengthened the SNR and amplitude equalization of the results through iterations, and successfully applied it to the processing of 3D data through phase coding (Dai et al., 2010). In recent years, many scholars have also studied LSRTM in complex media. Dai et al. (2015) implemented LSRTM based on viscoelastic media to compensate for phase distortion and energy attenuation caused by acoustic hypothesis. The results of the numerical test indicate that this algorithm has good effect in resolution enhancement and removing artifacts. Ren et al. (2017) proposed the LSRTM in elastic media, calculated the elastic demigration operator through Born approximation, and then used the Lagrange multiplier to obtain the adjoint equation in order to get the gradient to reflectivity. The final results show that this method reduces the dependence on initial speed and enhances the anti-noise ability. Considering the influence of anisotropy on the final imaging results, Huang et al. (2016) extended LSRTM to VTI media, and introduced the plane-wave coding strategy into the inversion framework to reduce I/O requirements and improve inversion efficiency.

The main advantage of LSRTM is removal of low frequency noise. For high-frequency noise, such as high-order scattering artifact and multiple artifact, LSRTM is difficult to eliminate (Lin et al., 2020). Consequently, special methods need to be introduced to eliminate such interference. These high-frequency noises will cause errors in forward modeling. In order to suppress high-order scattering, wavefield reconstruction inversion (WRI) method can be introduced into LSRTM. This method is created by van Leeuwen and Herrmann (2013) to incorporate errors into inversion. WRI method can reform the objective function and update gradient by taking the wave equation as a constraint, optimize the inversion process to avoid the solution process plunging into local mínimum (Li et al., 2017; Lin et al., 2018).

This paper will first review the forward modeling basic theory of stable qP-wave equation, further introduce this method into LSRTM, and compare and analyze the influence of LSRTM methods based on different media assumptions on imaging in TTI media. Then, we will deduce the theoretical

framework of wavefield reconstructed LSRTM in TTI media, and take numerical tests to verify the validity of the method.

THEORY

Review of stable pure qP-wave equation in TTI media

Alkhalifah (2000) derived the fourth-order qP-wave equation in VTI media under the acoustic approximation. Considering the difficulty of solution, the equation can be reduced to the first-order velocity-stress equation. When the isotropic symmetry axis tilts, that is, the media become TTI media, the first-order velocity-stress equation is too complex to be implemented by finite difference (FD) method. Therefore, the fourth-order partial differential equation (PDE) is reduced to the second-order coupled qP wave equation (Zhang et al., 2003). It has the advantages of simple form, easy implementation and convenient expansion to TTI media.

The second-order qP-wave equation in TTI media is

$$\begin{cases} \dfrac{\partial^2 p}{\partial t^2} = v_{px}^2 T_2 p + v_{pz}^2 T_1 q \\ \dfrac{\partial^2 q}{\partial t^2} = v_{pn}^2 T_2 p + v_{pz}^2 T_1 q \end{cases}, \tag{1}$$

$$\begin{aligned} T_1 = {} & \sin^2\theta\cos^2\theta\frac{\partial^2}{\partial x^2} + \sin^2\theta\sin^2\varphi\frac{\partial^2}{\partial x^2} + \cos^2\theta\frac{\partial^2}{\partial z^2} \\ & + \sin^2\theta\sin 2\varphi\frac{\partial^2}{\partial x\partial y} + \sin 2\theta\sin\varphi\frac{\partial^2}{\partial z\partial y} + \sin 2\theta\cos\varphi\frac{\partial^2}{\partial x\partial z} \end{aligned} \tag{2}$$

$$T_2 = \frac{\partial^2}{\partial x^2} + \frac{\partial^2}{\partial y^2} + \frac{\partial^2}{\partial z^2} - T_1 \quad , \tag{3}$$

where p and q are scalar wave fields, v_{px} and v_{pz} are P-wave reference velocity in the x-direction and z-direction, respectively, and v_{pn} is the P-wave NMO velocity.

Because the general pseudoacoustic approximation directly sets the vertical component of shear wave velocity as 0, the influence of shear wave velocity on the FD process is ignored. This leads to serious numerical instability in the process of wavefield propagation when the model parameters are extreme. Considering this problem, a smaller shear wave

velocity can be introduced to constrain the FD process. The equation can be expressed as

$$\begin{cases} \dfrac{\partial^2 p}{\partial t^2} = v_{px}^2 T_2 p + \left(v_{pn}^2 - v_{sz}^2\right) T_1 q + v_{sz}^2 T_1 p \\ \dfrac{\partial^2 q}{\partial t^2} = \left(v_{pz}^2 - v_{sz}^2\right) T_2 p + v_{pz}^2 T_1 q + v_{sz}^2 T_2 q \end{cases} . \tag{4}$$

The empirical formula can be represented as (Tsvankin, 2012)

$$v_{sz} = v_{pz}\sqrt{(\varepsilon - \delta)/\sigma} \quad , \tag{5}$$

where v_{sz} is the vertical velocity component of shear wave, ε and δ are Thompsen parameters. σ can be a constant of 0.9.

The modified coupled equation can effectively suppress the numerical instability, but due to the assumption of S-wave velocity, there will be obvious S-wave front in the wavefield. If the S-wave velocity field is inconsistent with the P-wave velocity field in structure, or there is no effective S-wave energy in the field data set, such S-wave field is very easy to form crosstalk in the imaging results, and it is difficult to eliminate it by iteration in LSRTM. In order to solve the limitations in application of coupled equations, Zhan et al. (2012) derived stable pure qP-wave equation

$$\frac{\partial^2 p}{\partial t^2} = v_{pz}^2 L p \quad , \tag{6}$$

$$\begin{aligned} L = {} & k_x^2 + k_z^2 + 2\cos^2\theta\left(\delta\sin^2\theta + \varepsilon(1+2\varepsilon)\cos^2\theta\right)\frac{k_x^4}{(1+2\varepsilon)k_x^2 + k_z^2} \\ & + 2\sin^2\theta\left(\delta\cos^2\theta + \varepsilon(1+2\varepsilon)\sin^2\theta\right)\frac{k_z^4}{(1+2\varepsilon)k_x^2 + k_z^2} \\ & + 2\sin 2\theta\left(\varepsilon(1+2\varepsilon) + \left(\varepsilon + 2\varepsilon^2 - \delta\right)\cos 2\theta\right)\frac{k_x^3 k_z}{(1+2\varepsilon)k_x^2 + k_z^2} \\ & + 2\sin 2\theta\left(\varepsilon(1+2\varepsilon) - \left(\varepsilon + 2\varepsilon^2 - \delta\right)\cos 2\theta\right)\frac{k_z^3 k_x}{(1+2\varepsilon)k_x^2 + k_z^2} \\ & + \frac{1}{2}\sin 2\theta\left(-3\varepsilon - 6\varepsilon^2 - \delta + 3\left(\varepsilon + 2\varepsilon^2 - \delta\right)\cos 2\theta\right)\frac{k_z^2 k_x^2}{(1+2\varepsilon)k_x^2 + k_z^2} \end{aligned} . \tag{7}$$

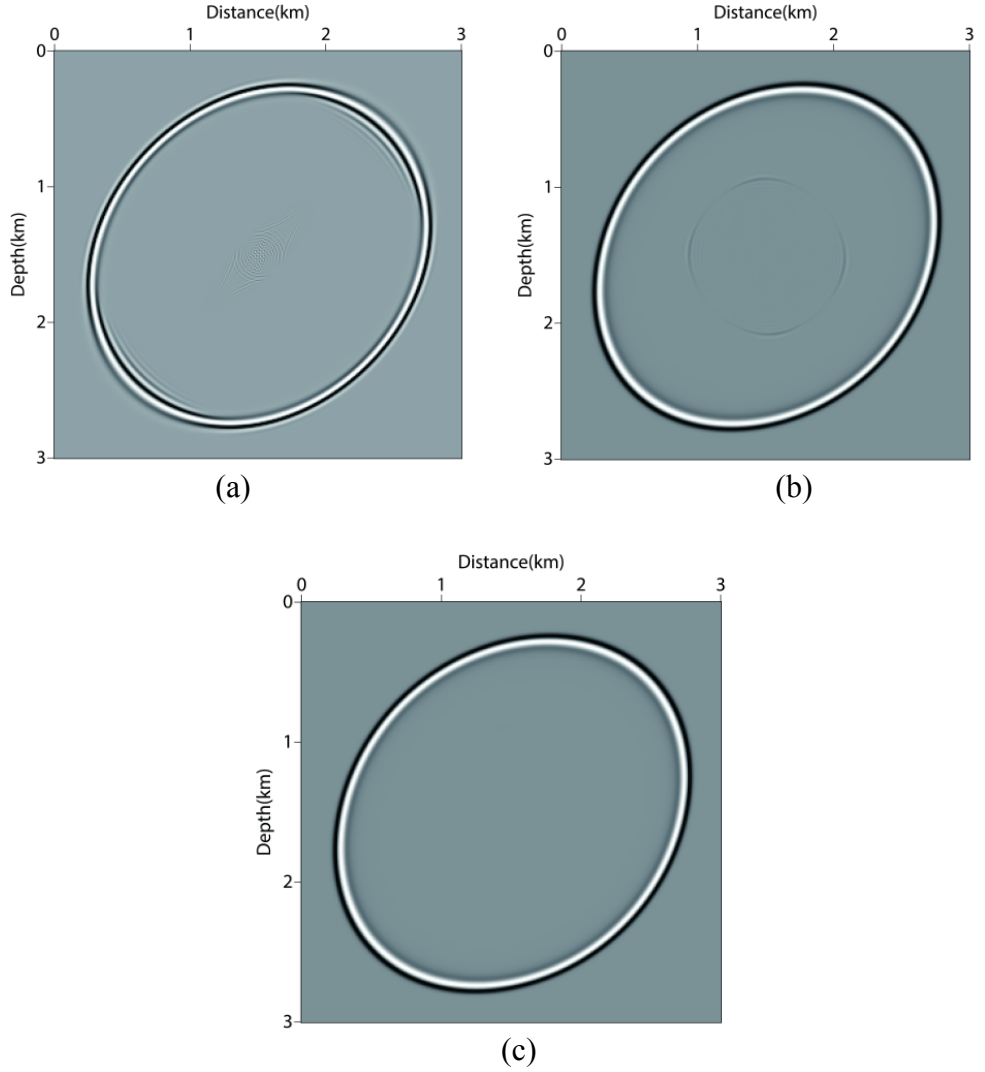

Fig. 1. Snapshots at 600 ms by (a) coupled qP-wave equation and (b) modified coupled qP-wave equation and (c) stable pure qP-wave equation.

We take numerical tests to verify the stability of stable pure qP-wave equation in TTI media. The tests use temporal second-order and spatial twelfth-order FD scheme. We build a 301×301 homogeneous model with grid interval of 10 m both in x- and z-direction. The velocity, ε , δ and polarization angle θ of the model are 2000 m/s, 0.25, 0.2 and 45 degrees respectively. We choose Ricker wavelet to simulate the source, the main frequency is 25 Hz, and the location of source is at point (151,151). The wavefield propagation time is 700 ms and the time interval is 1 ms. Fig.1(a) is calculated by original coupled qP-wave equation, there is serious numerical instability in the snapshot, accompanied by obvious shear wave interference. Fig. 1(b) is calculated by modified qP-wave equation which introduce the assumed shear wave velocity into second-order equation. This equation eliminate the numerical instability but result in a shear wavefield that can not be ignored during forward modeling or imaging. The snapshot of Fig. 1(c) shows a single visible wave front without obvious shear wave interference. The P-wave simulated by stable pure qP-wave equation effectively meet the requirement of imaging.

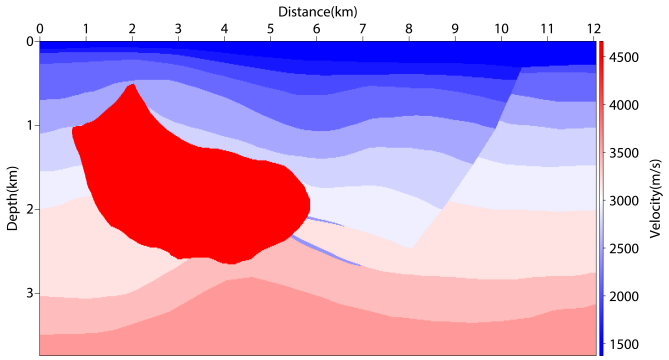

(a)

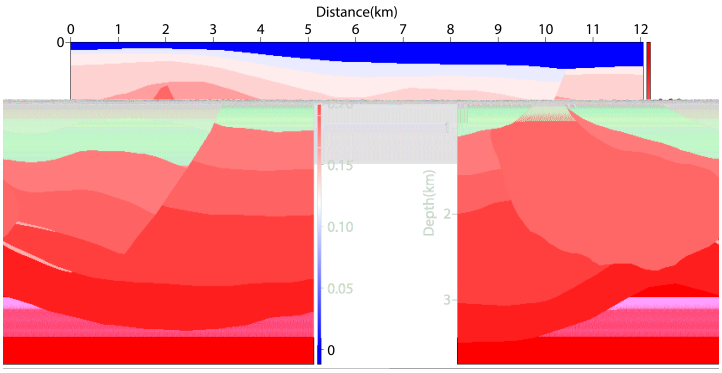

(b)

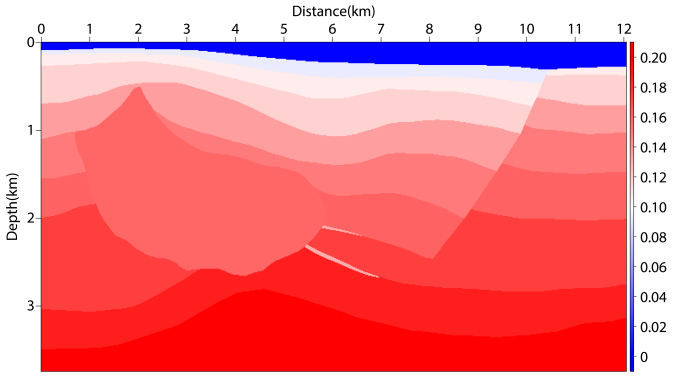

(c)

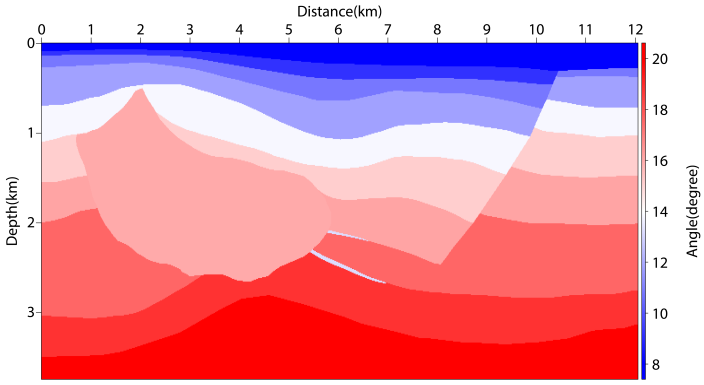

(d)

Fig. 2. Hess TTI model: (a) velocity, (b) ε , (c) δ , (d) polarization angle θ.

We test the adaptability of the stable pure qP-wave equation and observe the phenomena when conducting forward modeling in complex models. A set of 1206×375 Hess TTI model (Fig. 2) is selected for numerical test. The horizontal and vertical grid interval is 10 m. The total propagation time is 2000 ms with time interval of 1 ms. The main frequency of Ricker wavelet is 25 Hz. We intercept the snapshots at 1000 ms and 1500 ms in the two simulation methods respectively. Fig. 3(a) is a snapshot of the wavefield at 1000 ms using the coupling qP-wave equation. The wavefield at this time contains S-wave interference, and numerical instability can be observed locally. Fig. 3(b) shows the wavefield simulated by the same method at 1500ms. The numerical value is seriously unstable, and the order of magnitude reaches nearly 4000 times the effective wavefield, which has made the effective wavefield unable to be displayed. By comparing the above snapshots, Fig. 3(c) and Fig. 3(d) show good stability. There is no numerical instability and obvious S-wave interference in wavefield propagation, the order of magnitude basically remains stabilization. Such wavefield is more conducive to two-way wave migration.

Anisotropic Born scattering

In order to facilitate the derivation of scattering wave expression equation, we start from the stable pure qP-wave equation in time-space domain (Mu et al., 2020b):

$$\frac{1}{V_P^2}\frac{\partial^2 p}{\partial t^2} - L\cdot Pos(p) = s(x,z,t) \quad , \tag{8}$$

$$\begin{aligned} L = {} & 2\cos^2\theta\left(\delta\sin^2\theta + \varepsilon(1+2\varepsilon)\cos^2\theta\right)\frac{\partial^4}{\partial x^4} \\ & + 2\sin^2\theta\left(\delta\cos^2\theta + \varepsilon(1+2\varepsilon)\sin^2\theta\right)\frac{\partial^4}{\partial z^4} \\ & + 2\sin 2\theta\left(\varepsilon(1+2\varepsilon) + \left(\varepsilon+2\varepsilon^2-\delta\right)\cos 2\theta\right)\frac{\partial^4}{\partial x^2\partial z^2} \\ & + 2\sin 2\theta\left(\varepsilon(1+2\varepsilon) - \left(\varepsilon+2\varepsilon^2-\delta\right)\cos 2\theta\right)\frac{\partial^4}{\partial x^3\partial z} \\ & + \frac{1}{2}\sin 2\theta\left(-3\varepsilon-6\varepsilon^2-\delta+3\left(\varepsilon+2\varepsilon^2-\delta\right)\cos 2\theta\right)\frac{\partial^4}{\partial x\partial z^3} \end{aligned} \quad , \tag{9}$$

where Pos represents the Possion operator, which is used to solve the adjoint wavefield of scalar wavefield p. $s(x,z,t)$ indicates the source.

If the contribution of anisotropic parameters to scattering is ignored (Dutta and Schuster, 2014), that is, only the velocity field is decomposed by Born approximation, the wave equation can be further expressed as

$$\left(\frac{1}{V_{P0}^2}+\frac{1}{V_{P0}^2}\left(\frac{V_{P0}^2}{V_P^2}-1\right)\right)\frac{\partial^2 p}{\partial t^2}-L\cdot Pos(p)=s(x,z,t) \quad . \tag{10}$$

V_{P0} and V_P refer to the background velocity field and disturbed velocity field respectively.

The wavefield is linearized and decomposed into background wave field p_0 and scattering wavefield (Mu et al., 2020a), and the equation is expressed as

$$\left(\frac{1}{V_{P0}^2}+\frac{1}{V_{P0}^2}\left(\frac{V_{P0}^2}{V_P^2}-1\right)\right)\frac{\partial^2}{\partial t^2}(p_0+p_s)-L\cdot Pos(p_0+p_s)=s(x,z,t) \tag{11}$$

$$m(x)=\frac{1}{V_{P0}^2}\left(\frac{V_{P0}^2}{V_P^2}-1\right)\frac{\partial^2}{\partial t^2} \quad ,$$

is the definition of the scattering potential. We extract the equation of scattering wavefield

$$\frac{1}{V_{P0}^2}\frac{\partial^2}{\partial t^2}p_s-L\cdot Pos(p_s)=-m(\mathbf{x})p_0 \quad . \tag{12}$$

TTI-WRI-LSRTM

Wavefield reconstruction inversion is actually a strategy of adding penalty terms to unconstrained optimization problems to make them contain constraint information. This strategy uses the wave equation itself as a penalty term to broaden the solution search space and accelerate the convergence of the inversion problem (Lin et al., 2018). We add the scattering wave equation in TTI media as a constraint to the objective function of LSRTM (theory of TTI-LSRTM is shown in Appendix A), the information of scattering wave is fully considered in the inversion problem so that the high-order scattering artifacts caused by high-speed body can be reduced. First, we take a review of conventional LSRTM objective function:

$$J(m)=\frac{1}{2}\left\|d_{cal}-d_{obs}\right\|_2^2 \quad . \tag{13}$$

Considering the WRI inversion framework, the conventional objective function is extended, the scattering equation we derived is introduced as a constraint. The objective function is reconstructed to become a 2-norm function related to m and p_S:

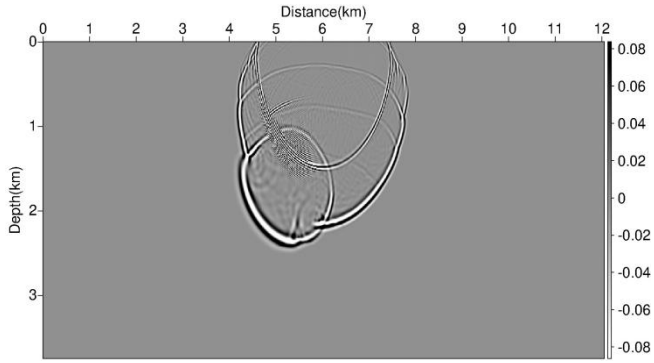

(a)

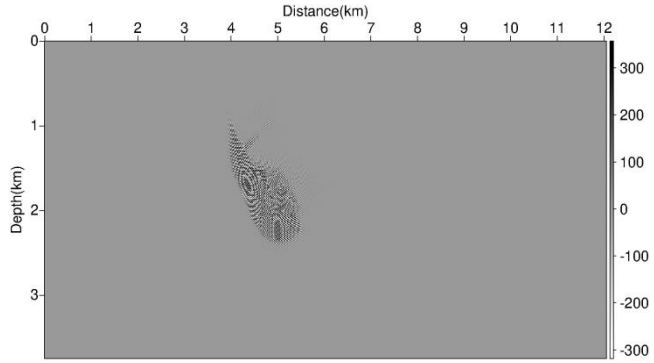

(b)

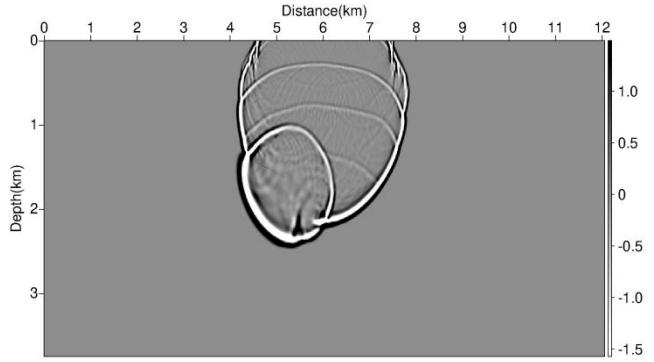

(c)

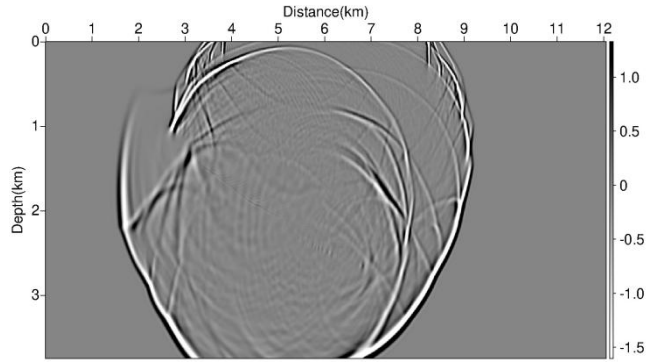

(d)

Fig. 3. Snapshots from modeling of Hess model: (a) at 1000 ms by coupled qP-wave equation, (b) at 1500 ms by coupled qP-wave equation, (c) at 1000 ms by stable pure qP-wave equation, (d) at 1500 ms by stable pure qP-wave equation.

$$J(m, p_s) = \frac{1}{2}\left\|\mathbf{L}p_s - d_{obs}\right\|_2^2 + \frac{\lambda}{2}\left\|A(m)p_s - m(\mathbf{x})p_0\right\|_2^2 \quad , \tag{14}$$

where $A(m) = \frac{1}{V_{P0}^2}\frac{\partial^2}{\partial t^2} - L \cdot Pos$ and λ is the constraint factor. The basis of the objective function can refer to Appendix B.

TTI-WRI-LSRTM

Wavefield reconstruction inversion is actually a strategy of adding penalty terms to unconstrained optimization problems to make them contain constraint information. This strategy uses the wave equation itself as a penalty term to broaden the solution search space and accelerate the convergence of the inversion problem (Lin et al., 2018). We add the scattering wave equation in TTI media as a constraint to the objective function of LSRTM (theory of TTI-LSRTM is shown in Appendix A), the information of scattering wave is fully considered in the inversion problem so that the high-order scattering artifacts caused by high-speed body can be reduced. First, we take a review of conventional LSRTM objective function:

$$J(m) = \frac{1}{2}\left\|d_{cal} - d_{obs}\right\|_2^2 \quad . \tag{13}$$

Considering the WRI inversion framework, the conventional objective function is extended, the scattering equation we derived is introduced as a constraint. The objective function is reconstructed to become a 2-norm function related to m and p_s:

$$J(m, p_s) = \frac{1}{2}\left\|\mathbf{L}p_s - d_{obs}\right\|_2^2 + \frac{\lambda}{2}\left\|A(m)p_s - m(\mathbf{x})p_0\right\|_2^2 \quad , \tag{14}$$

where $A(m) = \frac{1}{V_{P0}^2}\frac{\partial^2}{\partial t^2} - L \cdot Pos$ and λ is the constraint factor. The basis of the objective function can refer to Appendix B.

The new objective function contains two independent variables, which is not convenient to solve the gradient directly. Therefore, WRI can be mainly divided into two steps. The first step is to reconstruct the wavefield, and the second step uses the reconstructed wavefield to modify the gradient. Considering the linear relationship between the scattering wavefield and the scattering potential in the objective function, we gradually solve the reconstructed scattering wavefield by the following minimization problem:

$$J(p_s) = \left\| \begin{pmatrix} \mathbf{L} \\ \lambda A(m) \end{pmatrix} p_s - \begin{pmatrix} d_{obs} \\ \lambda m(\mathbf{x})p_0 \end{pmatrix} \right\|_2^2 \quad . \tag{15}$$

For this objective function, if the model parameters are known, we can give an extended state variable

$$\left(\lambda A(m)^T A(m) + \mathbf{L}^{\mathrm{T}}\mathbf{L}\right)p_s = \lambda A\left(m\right)^T + P^T d \quad . \tag{16}$$

In LSRTM, the scattering wave is obtained by demigration, which is essentially the forward modeling process (Wang et al., 2016) by introducing the reflectivity. Therefore, we can assume that the source of demigration is the product of the reflectivity and the background wavefield. Based on this assumption, let the scattering wavefield be the sum of the source and the disturbance generated by the source, then expand the expression of the scattering wavefield

$$p_s\left(\mathbf{x},t\right) = m\left(\mathbf{x}\right)p_0 + \hat{p}_s\left(\mathbf{x},t\right)/\lambda \quad , \tag{17}$$

Substitute eq. (17) into eq. (16) to obtain

$$\begin{aligned}\hat{p}_s\left(\mathbf{x},t\right) = {} & \lambda^2 A\left(m\right)^T m\left(\mathbf{x}\right)p_0 + \lambda\mathbf{L}^{\mathrm{T}}d_{obs} \\ & - \lambda\left(\lambda A\left(m\right)^T A\left(m\right) + \mathbf{L}^{\mathrm{T}}\mathbf{L}\right)m\left(\mathbf{x}\right)p_0\end{aligned} \quad . \tag{18}$$

In this way, we can get the reconstruction equation of scattering wavefield. Then, we use the equation to modify the traditional LSRTM gradient to

$$g\left(\mathbf{x}\right) = -\lambda\sum_{t}^{nt}\frac{\dfrac{\partial^2 p_0\left(\mathbf{x},t\right)}{\partial t^2}\left[A\left(m\right)p_s\left(\mathbf{x},t\right) - m\left(\mathbf{x}\right)p_0\right]}{{p_0}^2\left(\mathbf{x},t\right)} \quad . \tag{19}$$

After the improved gradient is obtained, we can adopt the conjugate gradient (CG) strategy (Nemeth et al., 1999) to gradually optimize the imaging results of LSRTM by iterations. Our workflow is shown in Fig. 4.

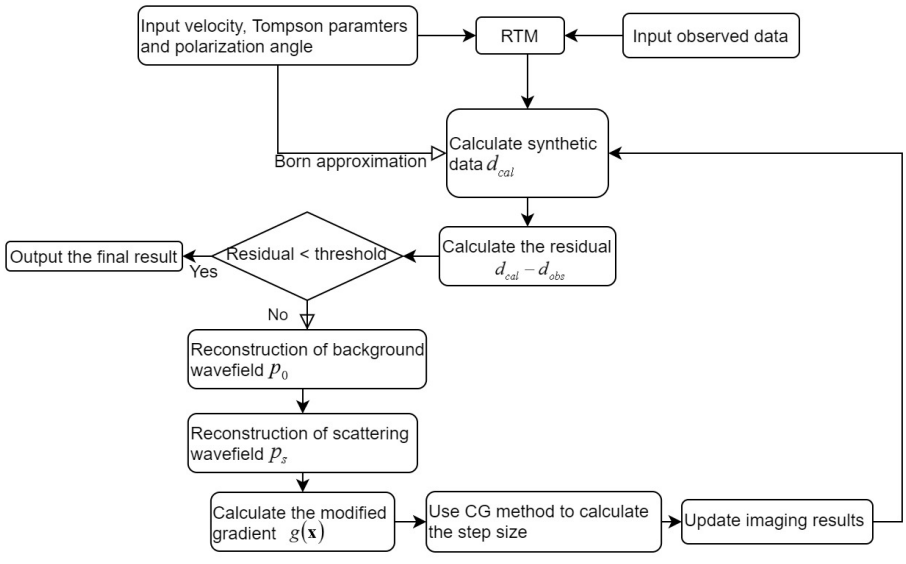

Fig. 4. Workflow of TTI-WRI-LSRTM.

Based on the method above, we develop the code following the algorithm:

TTI-WRI-LSRT

Input: velocity model, anisotropic parameters, polarization angle and shot data
Output: migration results after iterations
Initialize the iteration counter *iter* = 0
for *iter* < times of iterations
    Set shot counter is = 0
    for *is* < number of total shots
        Set time counter *it* = 0
        for it < total propagation time(forward)
            1.Forward modeling of wavefield by FD;
            2.Record wavefield at boundaries and save it in VRAM;
         it = *it* + 1;
        end for
        Set time counter *it* = total propagation time
        for it < total propagation time(backward)
            1.Read wavefield at boundaries which is saved in VRAM;
            2.Load wavefield at boundaries to reconstruct p_0 ;
            3.Backward modeling of observed data;
            4.Calculate $\hat{p}_s$ by eq. (18);
            5.Reconstruct the scattering wavefield p_s by eq. (17);
            6.Calculate gradient and update the migration results;
         it = *it* + 1;
        end for
    is = *is* + 1;
    end for
    for *is* < number of total shots(demigration)
        for *it* < total propagation time
              Calculate synthetic data
         it = *it* + 1;
        end for
    is = *is* + 1;
    end for
Calculate the misfit function
iter = *iter* + 1;
end for

To analyse the feasibility at GPU setting, it is necessary to estimate the occupied space in VRAM. The required VRAM space of our method and conventional LSRTM is shown below assuming the model size $nx \times nz$, total number of time points nt and number of shots ns:

Table 1. VRAM space required in TTI-LSRTM and TTI-WRI-LSRTM.

	TTI-WRI-LSRTM	TTI-LSRTM
Models	$4\times nx\times nz\times 4B$	$4\times nx\times nz\times 4B$
Forward wavefield	$6\times nx\times nz\times 4B$	$6\times nx\times nz\times 4B$
Backward wavefield	$6\times nx\times nz\times 4B$	$4\times nx\times nz\times 4B$
Wavefield at boundaries	$2\times nt\times(2\times nx+2\times nz)\times 4B$	$2\times nt\times(2\times nx+2\times nz)\times 4B$
Intermediate space for reconstruction	$5\times nx\times nz\times 4B$	0
Synthetic data	$2\times ns\times nt\times nx\times 4B$	$2\times ns\times nt\times nx\times 4B$
Migration results	$2\times nx\times nz\times 4B$	$nx\times nz\times 4B$
Total required memory (Example: Hess model in Figure 2, time points of 2800 and 100 shots)	2683M	2669M

According to the example in Table 1, the proposed method needs about 14M more VRAM space than the conventional method, and the VRAM requirements of both methods are significantly less than the maximum VRAM of the device we use. Therefore, we believe that such an increase in VRAM is acceptable for GPUs in most 2D cases.

Numerical test

We use the model with high-speed anomaly to carry out the numerical test. The first model is the Hess TTI model used above. We use this model to synthesize forward modeling records, conduct isotropic tests, VTI tests and TTI tests respectively, and observe the imaging results of different migration theories on observed data under TTI assumption. On the basis of TTI test, we continue to test WRI method to explore whether our method has practical effect on the imaging of high-speed anomalies and their surrounding structures. In addition, we test the field data of 2007 BP model(created by Hemang Shah and provided by BP Exploration Operation Company Limited) using TTI-LSRTM and TTI-WRI-LSRTM, and discuss the effect of this method on the actual data.

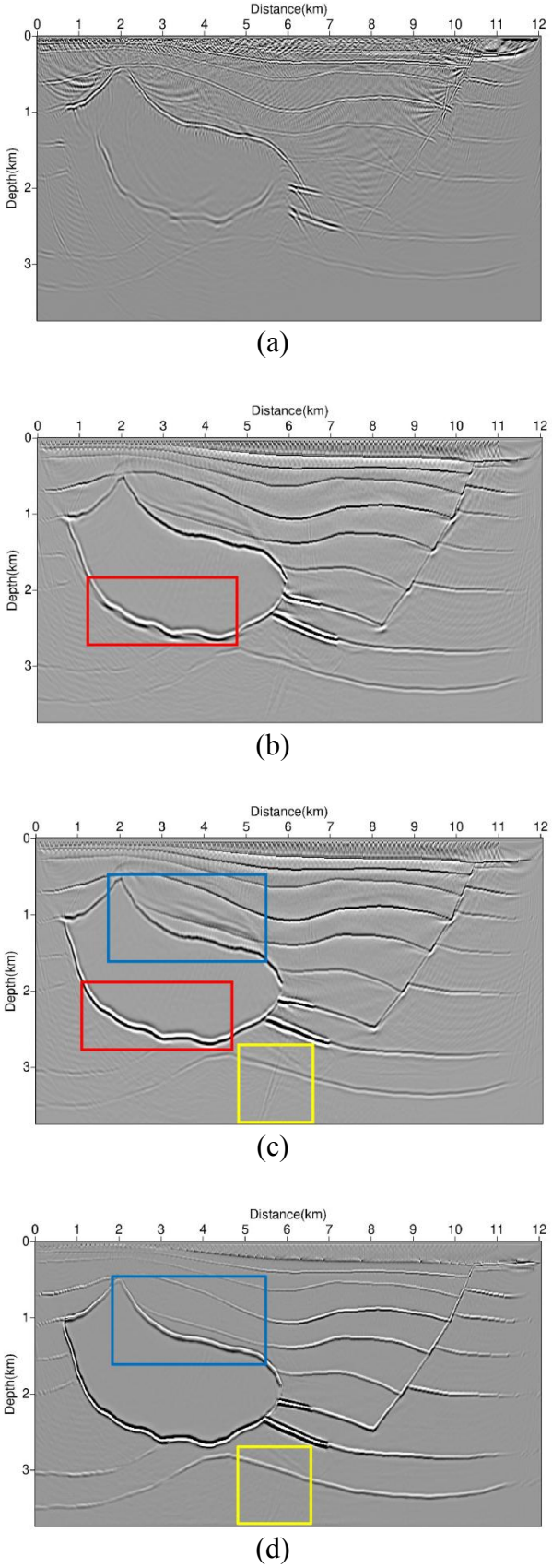

Fig. 5. LSRTM results of (a) isotropic P-wave equation, (b) VTI qP-wave equation, (c) TTI stable pure qP-wave equation and (d) TTI-WRI method after 20 iterations.

Fig. 5(a) is the result of LSRTM by isotropic P-wave equation. Because the shot record is simulated by anisotropic hypothesis, the isotropic equation can hardly propagate the observed wavefield backward accurately, resulting in low SNR of migration results. Such results are unable to effectively identify underground structures. Fig. 5(b) is the result of LSRTM by VTI qP-wave equation. Compared with isotropic migration, the accuracy and SNR of this result have been greatly improved, but there are still obvious artifacts in the region with large polarization angle [red box in Fig. 5(b)]. By introducing the TTI stable qP-wave equation, the artifacts are significantly weakened [red box in Fig. 5(c)], but the high-order scattering artifacts are still difficult to eliminate due to the existence of high-speed bodies [blue box and yellow box in Fig. 5(c)]. On the basis of TTI stable qP-wave equation, we can better eliminate the artifacts caused by high-order scattering wave [blue box and yellow box in Fig. 5(d)] through the wavefield reconstruction algorithm, the resolution and SNR are obviously improved.

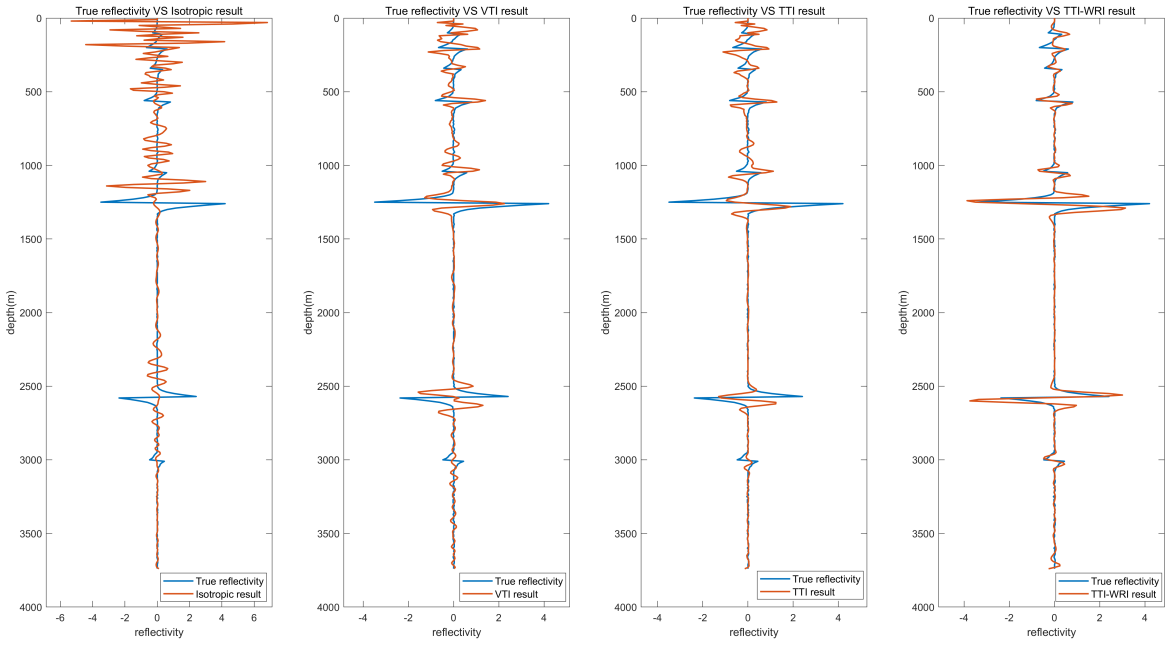

Fig. 6. Reflectivity verse LSRTM results at distance = 3500 m.

We extract the LSRTM data at distance = 3500 m for comparison (Fig.6). The isotropic results can hardly match the real reflectivity. The VTI results can roughly fit the real reflectivity at the upper part of the high-speed body, but due to enhancement of anisotropy, the imaging results in deep bear little resemblance to the real reflectivity. The LSRTM using TTI stable qP-wave theory shows good matching with the real reflectivity, but there is obvious high-order scattering artifacts between the depth of 700 m - 1000 m, and the resolution of the lower boundary of the high-speed body is also very limited. By introducing WRI theory, the optimized TTI-LSRTM enhances the SNR of imaging results and the resolution at the boundary of high-speed body, eliminates high-order scattering artifacts, and also improves the

imaging of structures under high-speed body. These improvements accelerate the convergence of residuals to a certain extent (Fig. 7).

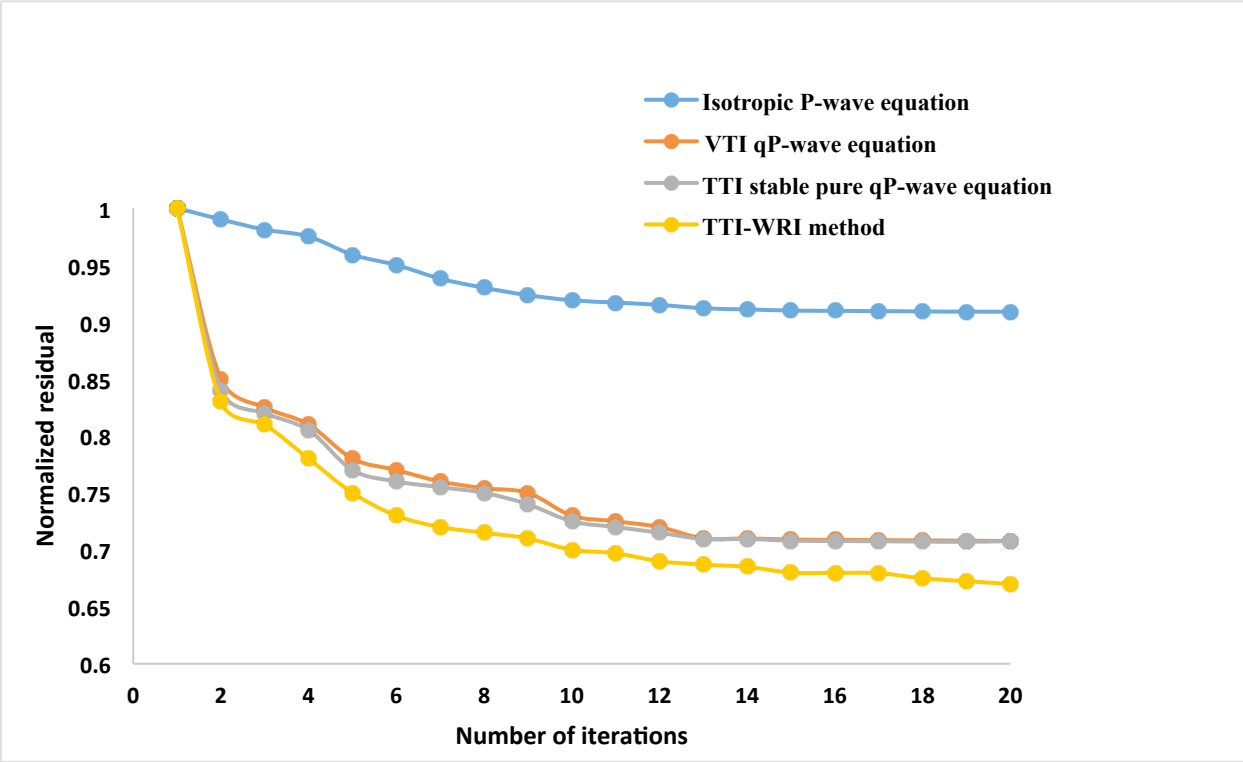

Fig. 7. Normalized residual curves of different migration methods.

It must be admitted that TTI-WRI-LSRTM is computationally more expensive than conventional TTI-LSRTM. The main calculation of LSRTM is concentrated at the solution of the wave equation. Compared with the conventional methods, the increase of the calculation in wavefield reconstruction algorithm mainly lies in the process of using the forward operator to reconstruct scattering wavefield.

Table 2. Run time of TTI-LSRTM and TTI-WRI-LSRTM.

	TTI-LSRTM	TTI-WRI-LSRTM
Device	NVIDIA Tesla K40c(12GB)	
Iterations	5	
Shots	100	
Run time(s)	20624	24708

To compare the computational efficiency of TTI-LSRTM and TTI-WRI-LSRTM, we record the run time after 5 iterations. The GPU device is NVIDIA Tesla K40c (12GB). The same test parameters as that in TTI Hess model test are used. Numerical tests show that the proposed method is more time-consuming than the conventional method (Table 2). For the Hess TTI model with 456250 grid points, the calculation time

increase rate is about 19%. Although the calculation cost increases, the migration result is significantly improved compared with that of conventional method. We are also striving to explore other optimized algorithms to reduce computing costs.

2007 BP Anisotropic model

This model is a common data set used to test TTI related methods. We still use CUDA computing platform for numerical test. The GPU model is NVIDIA Tesla K40c and the VRAM is 12 GB. Because the finite difference method has strong restrictions on the time sampling interval and spatial interval, the time sampling interval is changed from 8 ms to 1 ms by interpolation. Therefore, considering the limited VRAM and calculation time, we select 80 shots between fldr = 580 and fldr = 659 and their corresponding parameter field (Fig. 8) for testing.

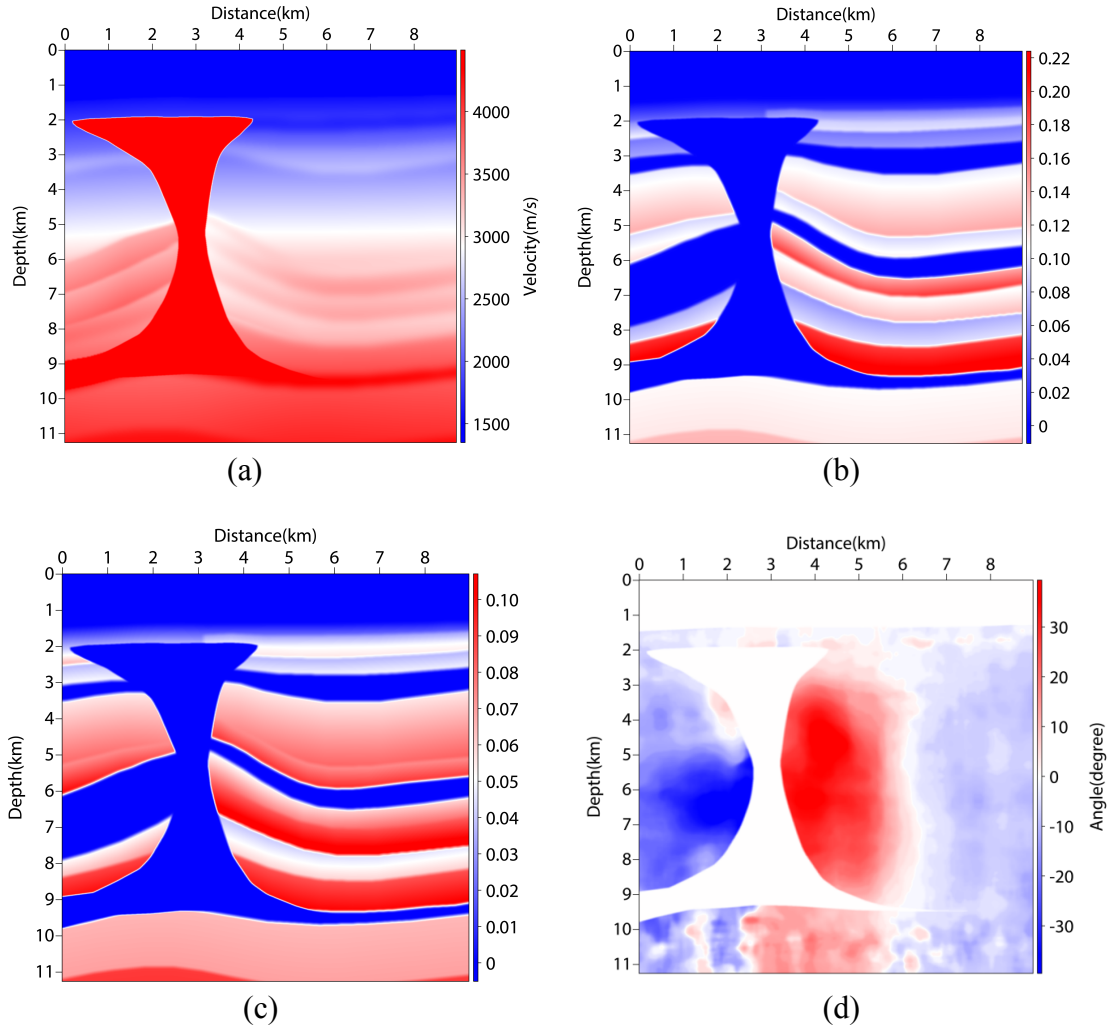

Fig. 8. 2007 BP anisotropic model: (a) P-wave velocity, (b) ε, (c) δ and (d) polarization angle θ.

The results show that the improved method further suppresses the high-order scattering artifacts around the high-speed body compared to

TTI-LSRTM, especially at the upper part of it (Fig. 9). TTI-WRI-LSRTM also has distinct advantages over the TTI-LSRTM method in depicting the boundary of high-speed body. In order to further observe whether the TTI-WRI method enhances the continuity of events by suppressing high-order scattering, we zoom the rectangular area within distance = 3450m - 4350 m and depth = 1875 m - 3387.5 m (Fig. 10). By the TTI-WRI method, the continuity of the events on the right side of the high-speed body is better than conventional TTI-LSRTM, which provides good data support for the identification of geological horizons.

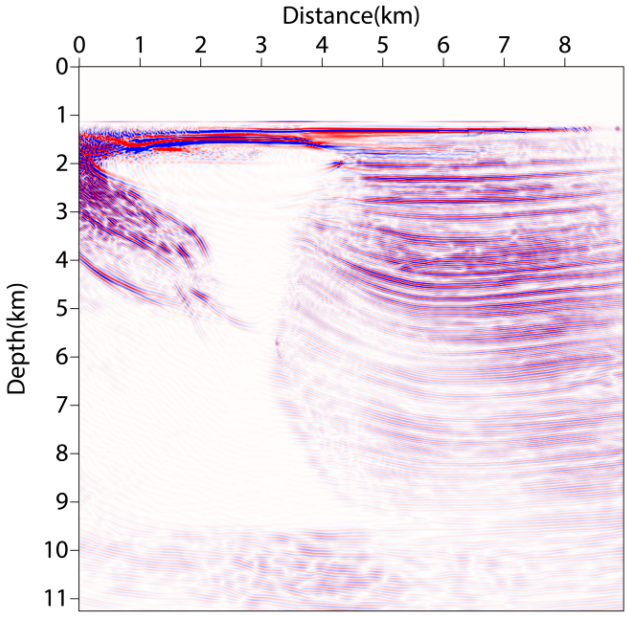

(a)

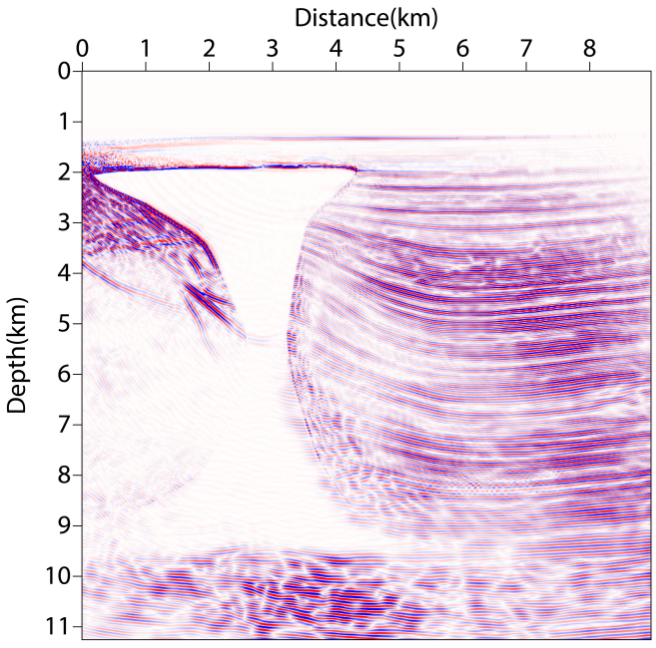

(b)

Fig. 9. (a) TTI-LSRTM and (b) TTI-WRI-LSRTM results of 2007 BP anisotropic model after 5 iterations.

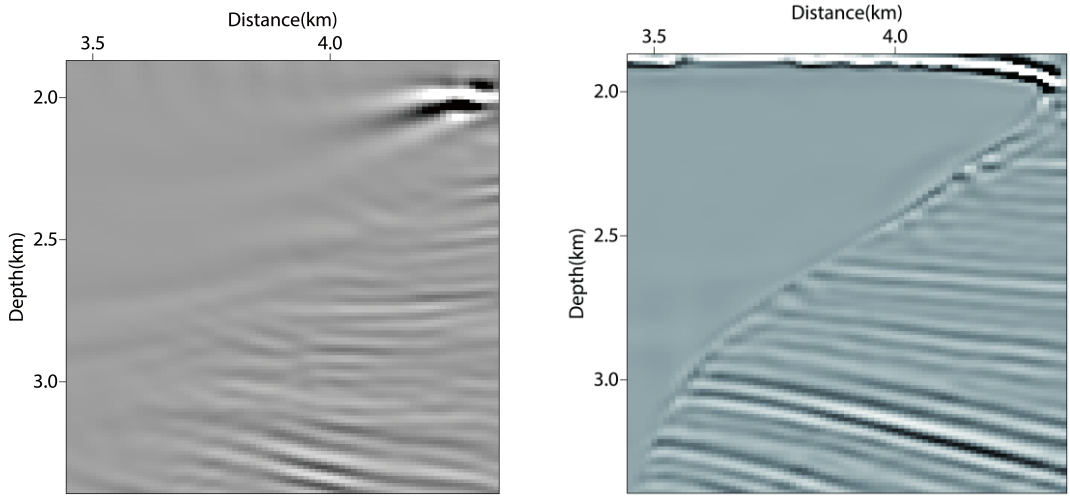

(a) (b)

Fig. 10. Enlargement of (a) TTI-LSRTM result and (b) TTI-WRI-LSRTM result within distance = 3450 m - 4350 m and depth = 1875 m - 3387.5 m.

CONCLUSION

In this paper, forward modeling tests are carried out to compare several propagation equations in TTI media. The stable pure qP-wave forward operator is selected as the propagator to realize TTI-LSRTM. By comparing the imaging results of TTI-LSRTM with isotropic LSRTM and VTI-LSRTM, the result of TTI-LSRTM matches better with the real reflectivity and has less artifacts. In order to solve the problem of scattering artifacts that is still existing in TTI-LSRTM, we derive the WRI algorithm of scattering waves in TTI media and apply it to LSRTM. Through the test of Hess model and 2007 BP field data, TTI-WRI-LSRTM shows a good ability for suppressing high-order scattering wave artifacts, and therefore accelerates the convergence of the objective function. Under the same number of iterations, the imaging result of TTI-WRI-LSRTM has higher SNR and resolution than that of the general TTI-LSRTM.

ACKNOWLEDGEMENT

This study is jointly funded by the National Natural Science Foundation of China's "Research on the inversion imaging method of viscoelastic parameters for deep lithologic reservoirs" (No. 42074133) and the China National Petroleum Corporation's "Study on Key Techniques of seismic velocity modeling and imaging of deep complex high steep structures and carbonate reservoirs in Tarim Basin" (No. ZD2019-183-003).

REFERENCES

Alkhalifah, T., 2000. An acoustic wave equation for anisotropic media. Geophysics, 65: 1239-1250.

Dai, W., Boonyasiriwat, C. and Schuster, G.T., 2010. 3D multi-source least-squares reverse time migration. Expanded Abstr., 80th Ann. Internat. SEG Mtg., Denver: 3120-3124.

Dai, W. and Schuster, G.T., 2013. Plane-wave least-squares reverse-time migration. Geophysics, 78(4): S165-S177.

Dai, W., Xu, Z. and Coates, R., 2015. Least-squares reverse-time migration for visco-acoustic media. Expanded Abstr., 85th Ann. Internat. SEG Mtg., New Orleans.

Dutta, G. and Schuster, G.T., 2014. Attenuation compensation for least-squares reverse time migration using the viscoacoustic-wave equation. Geophysics, 79(6): S251-S262.

Duveneck, E., Milcik, P., Bakker, P.M. and Perkins, C., 2008. Acoustic VTI wave equations and their application for anisotropic reverse time migration. Expanded Abstr., 78th Ann. Internat. SEG Mtg., Las Vegas: 3713.

Duveneck, E. and Bakker, P.M., 2011. Stable P-wave modeling for reverse-time migration in tilted TI media. Geophysics, 76(2): S65-S75.

Fletcher, R., Du, X. and Fowler, P.J., 2008. A new pseudo-acoustic wave equation for VTI media. Expanded Abstr., 78th Ann. Internat. SEG Mtg., Las Vegas.

Fletcher, R.P., Du, X. and Fowler, P.J., 2009a. Reverse time migration in tilted transversely isotropic (TTI) media. Geophysics, 74(6), WCA179.

Fletcher, R., Xiang, D. and Fowler, P.J., 2009b. Stabilizing acoustic reverse time migration in TTI media. Expanded Abstr., 79th Ann. Internat. SEG Mtg., Houston.

Fowler, P.J., Du, X. and Fletcher, R.P., 2010. Coupled equations for reverse time migration in transversely isotropic media. Geophysics, 75(1): S11-S22.

Grechka, V., Zhang, L. and Rector, J., 2004. Shear waves in acoustic anisotropic media. Geophysics, 69: 576-582.

Hestholm, S., 2009. Acoustic VTI modeling using high-order finite differences. Geophysics, 74(5): T67-T73.

Huang, J., Si, D., Li, Z. and Huang, J., 2016. Plane-wave least-squares reverse time migration in complex VTI media. Expanded Abstr., 86th Ann. Internat. SEG Mtg. Dallas.

Lambaré, G., Virieux, J., Madariaga, R. and Jin, S., 1992. Iterative asymptotic inversion in the acoustic approximation. Geophysics, 57: 1138-1154.

Li, Z., Lin, Y., Zhang, K., Li, Y. and Yu, Z., 2017. Time-domain wavefield reconstruction inversion. Appl. Geophys., 14: 523-528.

Lin, Y., Li, Z., Zhang, K. and Ding, R., 2020. Least-squares reverse time migration with first-order scattering wave equation penalty. Explor. Geophys., 52: 68-76. doi:10.1080/08123985.2020.1767503.

Lin, Y., Li, Z., Zhang, K. and Li, Y., 2018. Time domain wavefield reconstruction inversion based on new penalty scalar algorithm. Chinese J. Geophys. – Chin. Ed., 61: 4100-4109. doi: 10.6038/cjg2018L0760.

Mu, X., Huang, J., Yang, J., Guo, X. and Guo, Y., 2020a. Least-squares reverse-time migration in TTI media using a pure qP-wave equation. Geophysics, 85(4): S199-S216.

Mu, X., Huang, J., Yong, P., Huang, J. and Hu, Z., 2020b. Modeling of pure qP- and qSV-waves in tilted transversely isotropic media with the optimal quadratic approximation. Geophysics, 85(2): C71- C89.

Nemeth, T., Wu, C. and Schuster, G.T., 1999. Least-squares migration of incomplete reflection data. Geophysics, 64: 208-221.

Plessix, R.E., 2006. A review of the adjoint-state method for computing the gradient of a functional with geophysical applications. Geophys. J. Roy. Astron. Soc., 167: 495-503.

Ren, Z., Liu, Y. and Sen, M., 2017. Least-squares reverse time migration in elastic media. Geophys. J. Internat., 208: 1103-1125. doi: 10.1093/gji/ggw443.

Tarantola, A., 1984. Inversion of seismic reflection data in the acoustic approximation. Geophysics, 49: 1259-1266.

Tarantola, A., 2005. Inverse Problem Theory and Methods for Model Parameter Estimation. SIAM, Philadelphia. doi:10.1137/1.9780898717921.

Tsvankin, I., 2012. Seismic Signatures and Analysis of Reflection Data in Anisotropic Media, 3rd ed. SEG, Tulsa, OK. 10.1190/1.9781560803003, 431-438.

Uhsenbach, C. and Bale, R., 2009. TTI wave-equation migration for Canadian foothills depth imaging. The Leading Edge, 28: 1344-1355.

van Leeuwen, T. and Herrmann, F.J., 2013. Mitigating local minima in full-waveform inversion by expanding the search space. Geophys. J. Internat., 195: 661-667.

Wang, C., Yingst, D., Farmer, P. and Leveille, J., 2016. Full-waveform inversion with the reconstructed wavefield method. Expanded Abstr., 86th Ann. Internat. SEG Mtg., Dallas.

Zhan, G., Pestana, R.C. and Stoffa, P.L., 2012. Decoupled equations for reverse time migration in tilted transversely isotropic media. Geophysics, 77(2): T37-T45.

Zhang, Y., Zhang, G. and Bleistein, N., 2003. True amplitude wave equation migration arising from true amplitude one-way wave equations. Inverse Probl., 19: 1113.

Zhang, H., Yu, Z. and Zhang, G., 2011. A stable TTI reverse time migration and its implementation. Geophysics, 76(3): WA3-WA11.

Zhou, H., Zhang, G. and Bloor, R., 2006. An anisotropic acoustic wave equation for modeling and migration in 2D TTI media. Expanded Abstr., 76th Ann. Internat. SEG Mtg., New Orleans.

APPENDIX A

The theory of wavefield backward propagation can be deduced from the adjoint state method (Plessix, 2006). We define the adjoint variable p^*, and the migration equation can be written as

$$\frac{1}{V_0^2}\frac{\partial^2 p^*}{\partial t^2} - L\cdot Pos\left(p^*\right) = d_{adj} \quad , \tag{A-1}$$

$$\begin{aligned} L = {} & 2\cos^2\theta\left(\delta\sin^2\theta + \varepsilon\left(1+2\varepsilon\right)\cos^2\theta\right)\frac{\partial^4}{\partial x^4} \\ & + 2\sin^2\theta\left(\delta\cos^2\theta + \varepsilon\left(1+2\varepsilon\right)\sin^2\theta\right)\frac{\partial^4}{\partial z^4} \\ & + 2\sin 2\theta\left(\varepsilon\left(1+2\varepsilon\right) + \left(\varepsilon+2\varepsilon^2-\delta\right)\cos 2\theta\right)\frac{\partial^4}{\partial x^2\partial z^2} \\ & + 2\sin 2\theta\left(\varepsilon\left(1+2\varepsilon\right) - \left(\varepsilon+2\varepsilon^2-\delta\right)\cos 2\theta\right)\frac{\partial^4}{\partial x^3\partial z} \\ & + \frac{1}{2}\sin 2\theta\left(-3\varepsilon-6\varepsilon^2-\delta+3\left(\varepsilon+2\varepsilon^2-\delta\right)\cos 2\theta\right)\frac{\partial^4}{\partial x\partial z^3} \end{aligned} \quad , \tag{A-2}$$

where d_{adj} represents the adjoint source, that is the residual between the simulated wavefield and the observed wavefield.

The reverse time migration process of adjoint wavefield can be expressed in the form of gradient

$$g\left(\mathbf{x}\right) = \sum_{t}^{nt}\frac{\frac{\partial^2 p_0\left(\mathbf{x},t\right)}{\partial t^2}p^*}{{p_0}^2\left(\mathbf{x},t\right)} \quad . \tag{A-3}$$

Using the conjugate gradient algorithm, the update step length is calculated through the following steps

$$\beta = \frac{g^{k+1}\left(\mathbf{x}\right)^T g^{k+1}\left(\mathbf{x}\right)}{g^{k}\left(\mathbf{x}\right)^T g^{k}\left(\mathbf{x}\right)} \quad , \tag{A-4}$$

$$z^{k+1} = g^{k+1} + \beta z^k \quad , \tag{A-5}$$

$$\alpha = \frac{\left(z^{k+1}\right)^T g^{k+1}}{\left(Lz^{k+1}\right)^T\left(Lz^{k+1}\right)} \quad . \tag{A-6}$$

The gradient update equation is given

$$m^{k+1} = m^k + \alpha g^k \quad . \tag{A-7}$$

Using the Born approximation and ignoring the disturbance of anisotropic parameter field, we can decompose the velocity field and wavefield

$$V = V_0 + V_s \quad , \tag{A-8}$$

$$p = p_0 + p_s \quad . \tag{A-9}$$

It is assumed that the source of the disturbance field is a combination of the background field and the migration result of last iteration, then we can derive the qP-wave demigration equation of TTI-LSRTM from the pure qP-wave equation in TTI media

$$\frac{1}{V^2}\frac{\partial^2 p_s}{\partial t^2} - L \cdot Pos(p_s) = \frac{2v_s}{{v_0}^3}\frac{\partial^2 p_0}{\partial t^2} \quad . \tag{A-10}$$

$$\begin{aligned} L = {} & 2\cos^2\theta\left(\delta\sin^2\theta + \varepsilon(1+2\varepsilon)\cos^2\theta\right)\frac{\partial^4}{\partial x^4} \\ & + 2\sin^2\theta\left(\delta\cos^2\theta + \varepsilon(1+2\varepsilon)\sin^2\theta\right)\frac{\partial^4}{\partial z^4} \\ & + 2\sin 2\theta\left(\varepsilon(1+2\varepsilon) + \left(\varepsilon + 2\varepsilon^2 - \delta\right)\cos 2\theta\right)\frac{\partial^4}{\partial x^2\partial z^2} \\ & + 2\sin 2\theta\left(\varepsilon(1+2\varepsilon) - \left(\varepsilon + 2\varepsilon^2 - \delta\right)\cos 2\theta\right)\frac{\partial^4}{\partial x^3\partial z} \\ & + \frac{1}{2}\sin 2\theta\left(-3\varepsilon - 6\varepsilon^2 - \delta + 3\left(\varepsilon + 2\varepsilon^2 - \delta\right)\cos 2\theta\right)\frac{\partial^4}{\partial x\partial z^3} \end{aligned} \quad . \tag{A-11}$$

APPENDIX B

Combined with Tarantola's inversion method (2005), the basis of WRI theory is given here. Assuming that the model parameters are a-priori information, we can give the Gaussian distribution function of the wavefield

$$f(d \mid m) = \frac{1}{\sqrt{2\pi}\sigma_p} \exp\left(-\frac{1}{2} (A(m)u - q)(\sigma_p{}^2)^{-1} (A(m)u - q) \right) \quad . \tag{B-1}$$

Similarly, the Gaussian distribution function can be given to represent the measurement error

$$f(d) = \frac{1}{\sqrt{2\pi}\sigma_m} \exp\left(-\frac{1}{2} (Lp - d)(\sigma_m{}^2)^{-1} (Lp - d) \right) \quad . \tag{B-2}$$

Combining the probability density of measurement error and observation information, a posteriori state expression is given

$$\phi(m) = f(d \mid m) * f(d) \quad . \tag{B-3}$$

Ignoring the constant term, then we can get a maximum a posteriori probability estimate problema

$$\phi(m) = \exp\left(-\frac{1}{2} (A(m)u - q)(\sigma_p{}^2)^{-1} (A(m)u - q) \right) \exp\left(-\frac{1}{2} (Lp - d)(\sigma_m{}^2)^{-1} (Lp - d) \right) \tag{B-4}$$

Then the problem of solving the maximum probability density can be equivalent to the minimization problem in the form of eq. (14).